Applied Catalysis B: Environmental 239 (2018) 245–253

Contents lists available at ScienceDirect

Applied Catalysis B: Environmental

journal homepage: www.elsevier.com/locate/apcatb

Extracellular bacterial inactivation proceeding without Cu-ion release: Drastic effects of the applied plasma energy on the performance of the Cu-polyester (PES) samples

S. Rtimi[a,b,*], S. Konstantinidis[c], N. Britun[c], M. Bensimon[d], I. Khmel[e], V. Nadtochenko[f]

[a] Ecole Polytechnique Fédérale de Lausanne, EPFL-SB-ISIC-GPAO, Station 6, CH-1015, Lausanne, Switzerland
[b] Ecole Polytechnique Fédérale de Lausanne, EPFL-STI-LTP, Station 12, CH-1015, Lausanne, Switzerland
[c] Chimie des Interactions Plasma-Surface, Université de Mons, Place du parc 23, 7000 Mons, Belgium
[d] Ecole Polytechnique Fédérale de Lausanne, EPFL-ENAC-IIEGR-CEL, Bat GC, Station 18, CH-1015, Lausanne, Switzerland
[e] Institute of Molecular Genetics, Russian Academy of Sciences, Kurchatov Sq. 2, 123182, Moscow, Russia
[f] Institute of Chemical Physics, Russian Academy of Sciences, Kosigin str. 4, Moscow 119991, Russia

ARTICLE INFO

Keywords:
Cu-sputtered surfaces
Genetically modified bacteria
Photocatalysis
Redox
Catalysis
HIPIMS/DCMS

ABSTRACT

The widely different effects of Cu-polyester (PES) sputtered by high power impulse magnetron sputtering (HIPIMS) compared to the lower energy direct current magnetron sputtering (DCMS) leading to bacterial inactivation are addressed during the course of this study. The amounts of Ar^+ and Cu^+/Cu^{2+}-ions generated by HIPIMS (20 A) in the plasma was about five times the amounts detected when using for DCMS (0.3 A), but the relative distribution of these three ionic-species was similar. HIPIMS sputtered Cu-polyester (Cu-PES) at 20 A did not release Cu-ions after a few bacterial inactivation cycles but still lead to complete *E. coli* inactivation. Unambiguous separation of the intracellular Cu-ions effects and of the extracellular surface-contact was possible comparing the inactivation of wild *E. coli* to the inactivation of genetically modified porinless *E. coli*. The optical properties and sample microstructure of the Cu-PES samples were determined by diffuse reflectance spectroscopy (DRS) and by scanning transmission electron microscopy (STEM-HAADF). High-density films were obtained by HIPIMS in contrast to the low-density films prepared by DCMS. The DCMS sputtered Cu-PES presented large amounts of O-interstitial voids. A redox mechanism in bacterial inactivation was detected by X-ray photoelectron spectroscopy (XPS) by monitoring the Cu(I)Cu(II) species within the bacterial inactivation time.

1. Introduction

Copper, Cu-oxides and Cu- complexes have been utilized as effective materials for sterilizing liquids, textiles and surfaces due to their high cytotoxicity per unit weight. Cu is currently investigated in the formulation of more advanced surfaces leading to micro-organisms inactivation [1–10]. In addition, the use of supported Cu-nanoparticles (Cu-NPs) has been shown to be effective in precluding infections in implants/prostheses [11–13]. The excessive use of antibiotics is increasing the resistance of highly infectious microorganisms to drugs/antibiotics. This leads to the rise of hospital-acquired infections (HAIs). Due to this, research on Cu-NPs grafted on 2D and 3D-surface/catheters have experienced a rapid increase in the last decade in health-care facilities [14–19]. Cu/Cu-ions/Cu-surfaces containing highly disperse Cu have been reported by several groups. Gedanken et al., developed sonolysis method to fix the NPs on textiles [20,21]. Santos et al., recently reported consistent work on the bacterial inactivation mechanism by Cu-NPs under different experimental conditions [22–24]. Pillai et al., addressed work on Cu-mediated disinfection providing insights into the mechanism of Cu-doped semiconductors catalysts [25–28]. Dionysiou contributed with studies on Cu-photocatalysts designed to enhance the visible light absorption of composites/substrates [29]. Amal et al., has addressed the size dependency of Cu/CuO NPs on the cytotoxicity and bacterial inactivation kinetics [30]. Vasilev described the role of Ag/Cu antibacterial nanoparticles in medical devices [31]; and finally, Akhavan et al. reported work on Cu-nanoparticle photocatalysts immobilized on SiO_2-surfaces improving the performance and dispersion of Cu-NPs [32]. SiO_2 layers protected organic surfaces from the corrosion induced by the TiO_2 photo-generated holes (h^+) [33]. This consideration also applies for Cu-oxides generating (h^+).

Colloidal Cu-formulations on non-heat resistant surfaces like textiles and polymer films do not resist calcination temperatures [2,34,35]. The

* Corresponding author at: Ecole Polytechnique Fédérale de Lausanne, EPFL-SB-ISIC-GPAO, Station 6, CH-1015, Lausanne, Switzerland.
E-mail address: sami.rtimi@epfl.ch (S. Rtimi).

https://doi.org/10.1016/j.apcatb.2018.08.024
Received 1 May 2018; Received in revised form 4 July 2018; Accepted 8 August 2018
Available online 09 August 2018

heating at relative low temperature Cu-dispersions leads to Cu-films that are non-uniform, non-reproducible, present low-adhesion to the substrate and can easily be wiped out by contact [36]. This problem has been overcome by applying physical vapor deposition (PVD) processes to deposit Cu by condensation of the Cu-vapors from precursors on the textile/polymer substrate positioned at a lower temperature in the reaction vessel [37]. The PVD approach does not need an annealing process to fix the Cu-particles on the substrate. The most common PVD processes are evaporation and sputtering. The latter can be operated at different modes. During the last years, magnetron sputtering gained attention due to the high uniformity and adhesion of the thin films, especially when operating in either of these two modes: a) direct current magnetron sputtering (DCMS) [38] and b) by the more recently developed high power impulse magnetron sputtering (HIPIMS) at temperatures ≤ 110–140 °C [39–41]. During the last eight years, our group has reported systematic, comprehensive and detailed work on the bacterial inactivation by Cu- and Ag-sputtered surfaces either by DCMS or HIPIMS on non-heat resistant commercial substrates. These surfaces present potential applications as innovative and more advanced disinfecting agents [42–46].

This study addresses: a) the features of Cu-PES samples sputtered at different energy levels, b) the surface properties of the Cu-sputtered samples, c) the stability of the Cu-PES surfaces leading to bacterial inactivation and finally d) a simplified mechanistic scheme for the Cu-PES mediated disinfection. Genetic modification of wild bacterial strain leading to porinless bacteria were used to identify the contribution of ions and/or the surface-contact effects on the bacterial inactivation kinetics.

2. Materials and methods

2.1. Cu-sputtering procedures on PES, plasma analysis, and measure of the film deposition rate

Copper films were sputtered by DCMS or by HIPIMS. The latter used a high-power pulsed voltage, repetition frequency and a sputtering time adapted to control the time-averaged power delivered to the plasma. Deposition in DCMS or HIPIMS mode was carried out at a time-averaged power of 100 +/- 10 W. The pulse duration was in the range of 10–50 µs, the target voltage ranged from 500 to 900 V. The applied target currents of 20, 40, 80, and 100 A were carefully monitored during the HIPIMS Cu-sputtering. The frequency was adapted to keep a power of ~100 W during the deposition. Several deposition runs were carried out for each sample and the duration of the Cu-sputtering was systematically set at 5, 10, 20 or 100 s.

The substrate used was polyester (PES) cloth. It is a polyester Dacron polyethylene terephthalate type 54 spun, plain weave ISO 105-F04 used for color fastness determinations.

The measurements were performed in a 30 L cylindrical stainless-steel magnetron chamber equipped with a balanced magnetron cathode furnished with a Cu-target 10 cm in diameter and sputtered at a pressure of 10^{-2} Torr. The base pressure was always < ~5×10^{-6} Torr. The deposition chamber was pumped continuously by a turbo pump backed by a rotary pump. Then Ar gas was introduced at 10 mTorr at a flow of 40 sccm (standard cubic centimeter per minute). The PES-samples were positioned 6 cm above the Cu-target. Cu-atoms were sputtered on the PES with an energy of 10 eV in that was ionized at 500 V. Under pressures < 1 Pa, metal ions are accelerated in the sheath, a zone where an electric field exists. The latter is located between the plasma and the surface to be coated. It will define to a large extent the energy of the Cu and Ar-ions i.e. the Ion Energy Distribution Function (IEDF) reaching the surface is provided by the mass spectrometry data. The generation of Cu-ions in the magnetron chamber occurs concomitantly with the generation of an equal number of electrons. This warrants the electro-neutrality of the sputtered films. The deposition rate, e.g. the film thickness obtained after a given deposition duration, was measured prior any deposition runs by performing cross sectional Scanning Electron Microscopy (SEM) analysis of Cu films deposited on a glass slide.

The total amount of ions and the ion energies during the sputtering were monitored using a mass spectrometer (Hiden HAL7-EQP1000 mass-energy analyzer). The orifice of the mass spectrometer was located at the position of sample during the deposition runs. The IEDF was recorded and the relative ion fractions of Ar^+, Cu^+ and Cu^{2+}-ions were determined as a function of the plasma parameters. The Cu-content of the Cu-PES samples was determined by XRF in a PANalytical PW2400 spectrometer and the data is reported din Supplementary Table S1.

2.2. Surface characterization of the Cu-samples by diffuse reflectance spectroscopy (DRS) and scanning transmission electron microscopy (STEM)

Diffuse reflectance spectroscopy (DRS) was carried out on a Perkin Elmer Lambda 900 UV-VIS-NIR spectrometer provided for with a PELA-1000 accessory at wavelength between 200–800 nm and a resolution of 1.0 nm. The absorption spectra of the samples were plotted in Kubelka-Munk (K/S) units. Irradiation of the samples was carried out in a cavity by way of an Osram Lumilux 18 W/827 actinic light (4.5 mW/cm^2 and emitting between 360 nm and 700 nm). The spectral features of this lamp are shown in Supplementary Fig. S1. This type of lamp is commonly used as an indoor light source.

Scanning transmission electron microscopy (STEM) was carried out by way of an FEI Osiris instrument operated at 200 kV with spot size of 5, dwell time 50 and real time 600 s for the Cu-PES samples sputtered by DCMS or HIPIMS. The sputtered Cu-PES samples were prepared for the STEM analysis by embedding the samples in epoxy resin 45359 Fluka. The samples were then cross-sectioned with an ultra-microtome (Ultracut E) at an angle at 35°. The high-angle annular dark field (HAADF) imaging was mapped by EDX. The Z-contrasted images were obtained by collecting the scattered electrons through the objective of the high-angle annular dark-field (HAADF) detector.

2.3. Bacterial inactivation evaluation by plate counting, preparation of porinless E. coli and fluorescence stereomicroscopy

An overnight culture of *E. coli* (usually 2–5 × 10^9 cells/ml) grown in a LB, solution diluted 1000-fold in saline solution (0.85% NaCl in distilled water). The bacteria were incubated in the dark under aerobic conditions. The 1% dilution was then transferred into a fresh Laura Bertani solution (LB) und the incubation extended up to 15 h until reaching the stationary phase. Then, 50 µl aliquots were placed on the plasma-treated (i.e. Cu coated) and untreated PES samples (~1.0 cm^2). At pre-selected times, the inoculated surface was washed and vortexed with a saline solution and the cell suspension was collected into an Eppendorf tube. To verify if no bacterial cells (or insignificant amounts of cells) remained on the surface, the fabrics were incubated on Agar-plate and incubated overnight. No bacterial growth was detected after washing the samples. Experiments were carried out in triplicate. A 100 µl bacterial suspension of the washed bacteria from the sample was seeded on a Petri dish plate count agar (PCA). The Agar-plates with the inoculated colonies where incubated at 37 °C for 24 h, then evaluated for their CFU-content. This proceeding follows the bacterial evaluation kinetics reported during the last few years [44,45]. The bacterial inactivation set up is shown in Supplementary Fig. S2.

E. coli mutant strains deficient in OmpF and OmpC porins were prepared according to protocols found in references [46,47]. This approach allowed to compare the bacterial inactivation kinetics induced by: (i) the Cu-ions able to penetrate inside the cell, or (ii) or by contact of the bacteria with the Cu-PES surface (from now as: surface-contact). The *E. coli K12* ATCC bacterial strain is isogenic with the TK 821 genetically modified porinless bacteria. Both bacteria contain genotypes that reproduce indefinitely and remain similar for many generations.

The culture conditions used for the *E. coli* and the genetically modified *E. coli* were identical to limit the differences in growth of both strains.

Bacteria are able to scavenge and preclude ROS by the bacterial cytoplasm self-generated superoxide dismutase (SOD) and catalase (specific for the neutralization of H_2O_2). The four genes (katA, katE, katG and katX) expressing the catalase are different, which can influence their reaction pathway [48]. The katE and katG are the dominant catalase species as reported by Imlay [49]. The *E. coli* K12 and the genetically modified *E. coli* TK 821 were analyzed at the same growth phase. This is necessary due to changes introduced during the photocatalysis. The OD was monitored at 600 nm until it reached the exponential growth phase ~OD 0.6. The OD-values for both stains were observed to be similar indicating that the genetic differences do not influence the cell growth.

Fluorescence stereomicroscopy was carried out on samples inoculated with *E. coli* and incubated in a humidifier. A fluoro-chrome dye was used as the staining agent and received from Filmtracer™ (Live/Dead Biofilm Viability Kit from Molecular Probes, Invitrogem Co). The fluorescence of the samples was monitored in a Leica MZ16FA GmbH Wetzlar fluorescence stereomicroscope unit and the images were processed using the LAS vq.7.0 software. Adhesion of the bacteria (6×10^8 CFU/mL) to the PES was allowed for 2 min prior to the washing of the samples to remove the non-adherent bacteria.

2.4. Inductively-coupled mass spectrometry (ICP-MS) and X-ray Photoelectron Spectroscopy (XPS) of Cu-PES samples

Inductively coupled plasma spectrometry (ICP-MS) was used to assess the Cu corrosion occurring in the Cu-PES sample during bacterial disinfection. This allows the quantitative monitoring of the Cu-release during bacterial inactivation. The Finnigan™ ICP-MS unit was equipped with a double focusing reverse geometry mass spectrometer provided a detection limit of 0.2 ng/L (ppb). The washing solutions from Cu-PES samples were digested in nitric acid 69% (HNO_3: H_2O = 1: 1) to remove organics in solution, then the samples droplets were introduced into the ICP-MS unit. The Cu-content of the samples was subsequently quantified by mass spectrometry (MS).

The film X-ray photoelectron spectroscopy (XPS) was carried out using an AXIS NOVA photoelectron spectrometer (Kratos Analytical, Manchester, UK) provided for with a monochromatic AlKα $h\nu$ = 1486.6 eV) anode. The carbon C1s line with position at 284.6 eV was used as a reference to correct for the charging effects. The surface atomic percentage concentration was determined from the peak areas using the known sensitivity factors for each element [50]. Spectrum background subtraction and deconvolution was carried out according to Nogier et al., [51]. The deconvolution of the XPS-peaks was processed in a CasaXPS-Vision 2, from Kratos Analytical (UK). The Shirley background correction was applied to compensate for the shifts in the binding energies due to the electrostatic charging of the sample [52].

3. Results and discussion

3.1. Sputtering of Cu on PES textiles, profilometry and determination of the Cu-content of the Cu-coated samples

The film growth rate of Cu, as obtained during DCMS and HIPIMS experiments, was measured on glass plates prior to the Cu-deposition on PES (Table 1) to obtain reference images of the sputtered Cu-thicknesses. The Cu-content in the Cu-PES samples was determined was X-ray fluorescence (XRF) as shown in Supplementary Table S2.

Fig. 1a presents the total number of Cu-ions reaching the sample surface (the mass spectrometer is set at the location where PES samples are located during the thin film deposition runs and at the same floating potential) when sputtering Cu by DCMS or by HIPIMS. It is readily seen that population of Cu-ions and Ar-ions were maximized when HIPIMS sputtering was applied at 20 A/500 V. Fig. 1a shows that the HIPIMS sputtering at 20 A led to the highest number of ions compared to HIPIMS currents of 20, 80 and 100 A and DCMS sputtering applying 0.3 A. This observation is in line with previously reported data [38,39,52,53]. The higher ionization of Cu in the plasma phase induced through HIPIMS leads to an aggregation/coalescence of Cu-particles as shown below by way of HR-STEM.

Fig. 1a shows that the amount of Ar^+, Cu^+, Cu^{2+}-ions induced by the HIPIMS (20 A) was > 5 times the amount induced applying other currents. Fig. 1a shows that the Cu-ion present were maximized during HIPIMS-sputtering for 20 s at 20 A compared with other sputtering currents. The NPs uniformity, shape, size, layer thickness,

Table 1
Rate of the Cu-sputtering by DCMS or HIPIMS as determined by scanning electron microscopy (SEM) imaging of the film cross section.

Sputtering Type	Deposition rate (nm/min)
DCMS 0.3A	127
HIPIMS 20A	142
HIPIMS 40A	73
HIPIMS 80A	53
HIPIMS 100A	44

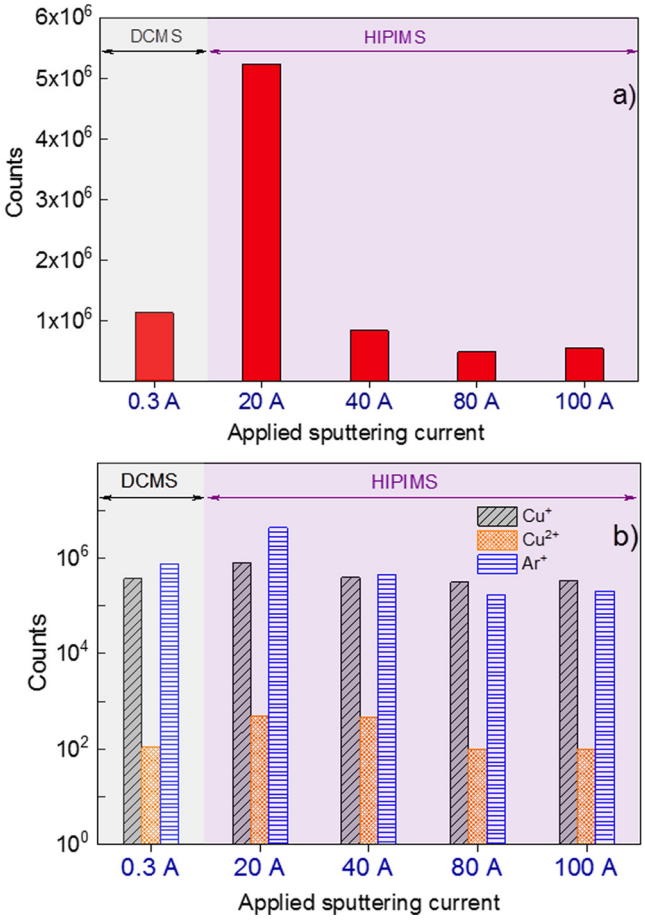

Fig. 1. a) Total ions counts in plasma phase during the deposition of Cu on PES for 20 s as detected by a mass spectrometer coupled to the magnetron sputtering unit. The DCMS-sputtering was carried out at 300 mA. Higher peak currents were used during HIPIMS process up to 100 A. Standard deviation of 10% for DCMS and 3% for HIPIMS deposition. **b)** Ion-species relative distribution in the plasma during the deposition of Cu on PES by DCMS and HIPIMS at different currents detected by the mass spectrometer coupled to the magnetron sputtering unit.

microstructure and features dependent on the number of layers deposited during the sputtering time. This controls the structure-reactivity relation of the Cu-catalyst clusters sputtered on the PES-substrate [37–40]. The thickness and microstructure of Cu are a function the applied sputtering current and lead to the significant difference in the total-ions count as shown in Fig. 1 [41]. S. Konstantinidis et al., reported on the diagnostics and understanding of the plasma-surface interaction in HIPIMS discharges. They followed the deposition rate of TiOx films deposited by HIPIMS as a function of the target peak current and the duty cycle and showed that the deposition rate increases until a certain current intensity then it decreases at higher applied currents [42]. This can explain the ions counts/distribution observed in Fig. 1a and b for the HIPIMS and DCMS deposed films correlated with their bactericidal activities.

Fig. 1b shows that the relative distribution of these three ionic-species was similar. Fig. 1b shows a higher percentage of Ar^+ when sputtering with HIPMS at 20 A. Three ionized species are shown in Fig. 1b. This ionic distribution led to different bacterial inactivation kinetics as shown below in Section 3.3. This suggests that a complex set of reactions intervene in processes leading to the production of species in the plasma phase and highlights the relation between the applied current and the relative species making-up the plasma. In addition, another important parameter that governs the thin film properties is the kinetic energy of the ions. The latter is much larger in HIPIMS-based process than in DCMS processes.

3.2. Surface characterization by DRS and STEM of Cu-samples sputtered by DCMS and HIPIMS

Fig. 2 shows the optical absorption spectra in Kubelka-Munk units for DCMS Cu-PES sputtered films for 20 s and for HIPIMS films sputtered for 20 s at different metal ion kinetic energies (different applied currents). The Cu-PES samples sputtered at 20 A and 100 A by HIPIMS show the highest diffuse reflectance absorption spectra consisting of Cu and Cu_2O species [7,55,56]. The optical absorption between 500 and 600 nm is attributed to the inter-band transition of Cu_2O. The absorption band between 600 and 720 nm has been assigned to the exciton band of the CuO d-d transition [36,57].

Fig. 3 shows the Cu and O mapping obtained by EDX using scanning transmission electron microscopy (STEM) mode. Fig. 3a presents the DCMS images for Cu-PES samples sputtered at 0.3 A. The Cu-atoms distribution (blue images) is seen to be dense and uniform. The O-species (green color at the right-hand side in Fig. 3) show large voids in the DCMS coated sample microstructure. These voids are due to O-interstitial species missing in the film central tract. Fig. 3b present the images for HIPMS Cu-PES samples sputtered for 20 s at 20 A. The main difference between the samples sputtered by HIPIMS and by DCMS was found in the film central tract as shown respectively in Fig. 3a and b. The oxygen distribution in the DCMS film shows more oxidized copper species in the bulk than the film prepared by HIPIMS. The latter showed more oxidized copper species at the topmost layers forming the interface with bacteria.

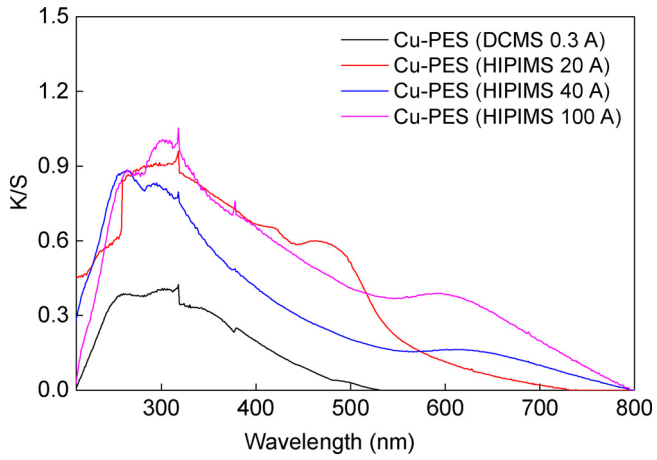

Fig. 2. Diffuse reflectance spectroscopy (DRS) of Cu-PES sputtered by DCMS and HIPIMS sputtered under different conditions as shown in the captions to Fig. 2.

The Cu-NPs with these sizes cannot penetrate into the bacteria core/cytoplasm through the cell wall porins with diameters of 1.0–1.3 nm [58]. In this case, the bacterial inactivation is due to the surface-contact between the Cu-PES samples and the bacteria cell envelope. It has been recently reported by Snaith et al. [59], that the size of metal-NPs plays a major role in charge transport within thin films. Cu with quantum size < 10 nm is made up by $\sim 10^4$ atoms [60]. The Cu-PES samples sputtered by HIPIMS shown in the right-hand side of Fig. 3b present a compact and continuous microstructure with no O-voids in the film central tract compared to the DCMS sputtered sample shown in Fig. 3a. This points to a significant difference in the microstructure of the or Cu-PES samples sputtered by HIPIMS compared to the DCMS samples.

3.3. Kinetics of wild E. coli K12 and genetically modified "porinless" E. coli inactivation on Cu-PES samples sputtered by DCMS and HIPIMS

Fig. 4 shows that Cu-PES samples coated by HIPIMS (20 A) lead to a faster *E. coli* inactivation compared with Cu-PES coated by DCMS (0.3 A) under light irradiation. Nonetheless, in the dark, the DCMS (0.3 A) sample lead to a faster bacterial inactivation compared to the HIPIMS (20 A) sample. The bacterial inactivation kinetics obtained by the HIPIMS 100 A sputtered sample was in experimental error with the data obtained for the 80 A sample. For this reason, the latter data it is not shown explicitly in Fig. 4.

In Fig. 4, the slow initial bacterial inactivation is seen to be followed by a faster bacterial inactivation step after ~20-30 min. At times shorter than 20–30 min, the damage to the cell-wall increased the cell-wall membrane permeability. This takes place during the induction period involving surface-contact effects due to the Cu-cytotoxicity. After this initial period, Cu-species/ions diffusion across the damaged cell-wall envelope proceeds leading to the complete bacterial inactivation [22]. Lu et al., [61] reported on the cell wall damages on thin films by atomic force microscopy (AFM) in conjugation with some other techniques leading to K+ ions release. Stoimenov et al., [62] also reported on AFM investigation of the cell membrane changes during photocatalytic exposure.

Fig. 4 shows that in the dark the bacterial inactivation by the DCMS sputtered samples proceeds more readily compared to HIPIMS sputtered samples. HIPIMS sputtered surfaces are more dense and compact compared to DCMS surfaces and therefore lead to a lower Cu-ion release. Work providing experimental evidence for this point was recently reported in reference [68]. Under light irradiation, Fig. 4 shows that HIPIMS-sputtered samples induced a faster bacterial inactivation compared with DCMS-samples. This is readily understood in terms of the behavior of the Cu-PES interaction with bacteria under light irradiation suggested below in Eqs. (1)–(6) generating reactive oxygen species (ROS) leading to bacterial cell wall lysis.

Fig. 5 presents the data for the light induced inactivation kinetics for normal *E. coli* K12 strains and for the genetically modified TK821 porinless bacteria on Cu-PES samples coated by HIPIMS (20 A) and for DCMS sputtered samples. Fig. 5, traces 1 and 2 follow the bacterial inactivation trend reported in Fig. 4. Fig. 5, traces 3 and 4 show a slower bacterial inactivation within 60 min for the genetically modified *E. coli* porinless bacteria on Cu-PES samples prepared by HIPIMS. The bacterial inactivation was observed to be slower occurring within 90 min on DCMS Cu-PES samples. This variance in the results found between Figs. 4 and 5 are due to the loss of bacterial cultivability (not detected by plate-count agar method reported in Fig. 4) without loss of viability. The reaction pH decreased within the bacterial disinfection

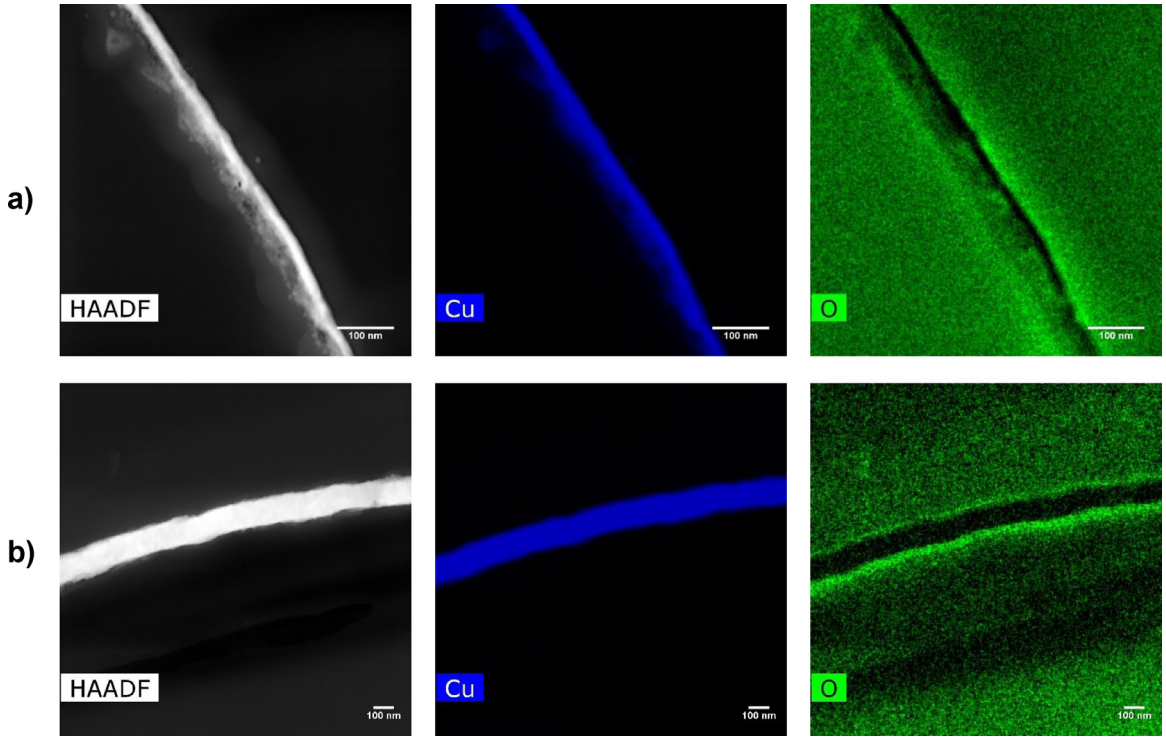

Fig. 3. High-angle annular dark field (HAADF) mapping of images obtained by scanning transmission electron microscopy (STEM) of the Cu-PES samples: a) sputtered by DCMS for 20 s at 0.3 A and b) sputtered by HIPIMS for 20 s at 20 A.

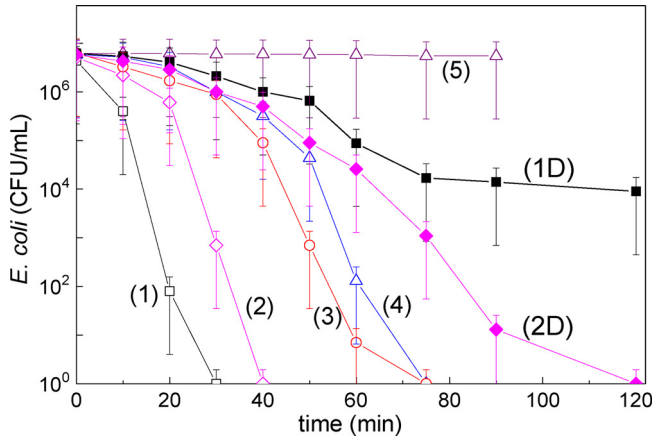

Fig. 4. *E. coli* (K 12) light activated bacterial inactivation on Cu-PES sputtered at different energies for 20 s on Cu-PES samples: (1) HIPIMS at 20 A, (2) DCMS at 0.3 A, (3) HIPIMS at 40 A, (4) HIPIMS at 80 A, and (5) un-sputtered PES under light irradiation by Osram Lumilux 18 W/827 actinic light (4.5 mW/cm^2), (1D) HIPIMS at 20 A in the dark and (2D) DCMS at 0.3 A in the dark.

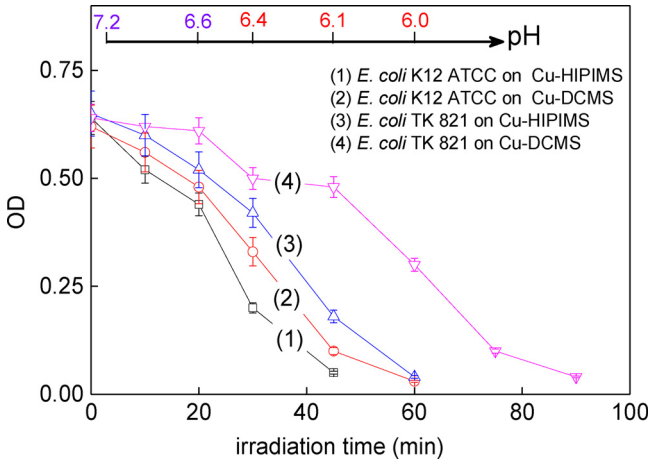

Fig. 5. OD 600 optical density of *E. coli* K12 ATCC cells: normal porins *E. coli* K12 (*ompR*$^+$ *ompF*$^+$*ompC*$^+$) versus porineless *E. coli* TK 821 (*ompR*$^+$ *ompF*$^-$ *ompC*$^-$) on Cu-PES samples sputtered by HIPIMS (20 A) and by DCMS(0.3 A). Runs on bacteria were carried out under Osram Lumilux 18 W/827 actinic light (4.5 mW/cm^2).

time from 7.2 to 6.0 (see in Fig. 5). Fenton-like processes leading to reactive oxygen species (ROS) have been reported by Fe-, Cu-, Cr-metal-ions [64]. Giannakis et al. [63], have recently reported work on the classical Fenton reactions involving Fe-ions in intracellular bacterial inactivation processes. Intracellular processes in *E. coli* K12 wild bacteria shown in Fig. 5 proceed faster compared with the genetically modified *E. coli* undergoing an initial extracellular surface-contact process. Intracellular processes involve Cu-ions diffusing through the damaged cell wall to the cell cytoplasm and leading to cell lysis/death [5,7,34,57].

A simplified mechanism for bacterial inactivation is suggested below in reactions (1–5). The effect of light leading to the bacterial cationic species in reaction (1) combined with the generation of H^+ in Eq. (2) rationalize thepH decrease from 7.2 to 6.0 in Fig. 5.

$$\text{Bacteria} + [\text{Cu-PES}] + \text{light} \rightarrow [\text{Cu*-PES}]\ \text{Bacteria} \rightarrow \text{Bacteria}^+ + [\text{Cu-PES}]\text{cbe}- \quad (1)$$

$$[\text{Cu-PES}]\ \text{vbh}^+ + \text{H}_2\text{Oads} \rightarrow \text{HO}^\circ\text{ads} + \text{H}^+ \quad (2)$$

$$[\text{Cu-PES}]\text{cbe-} + \text{O}_2 + \text{H}^+ \rightarrow \text{HO}_2\cdot\ E_0 - 0.05\ \text{NHE} \quad (3)$$

[65]

$$[\text{Cu-PES}]\text{cbe-} + \text{O}_2\text{ads} \rightarrow \text{O}_2\cdot - \text{ads}\ E_0 - 0.16\ \text{NHE} \quad (4)$$

[65]

$$[\text{Cu-PES}]\text{vbh}^+ + \text{OH} - \text{ads} \rightarrow \text{HO}^\circ\ E_0\ \text{-1.90 NHE} \quad (5)$$

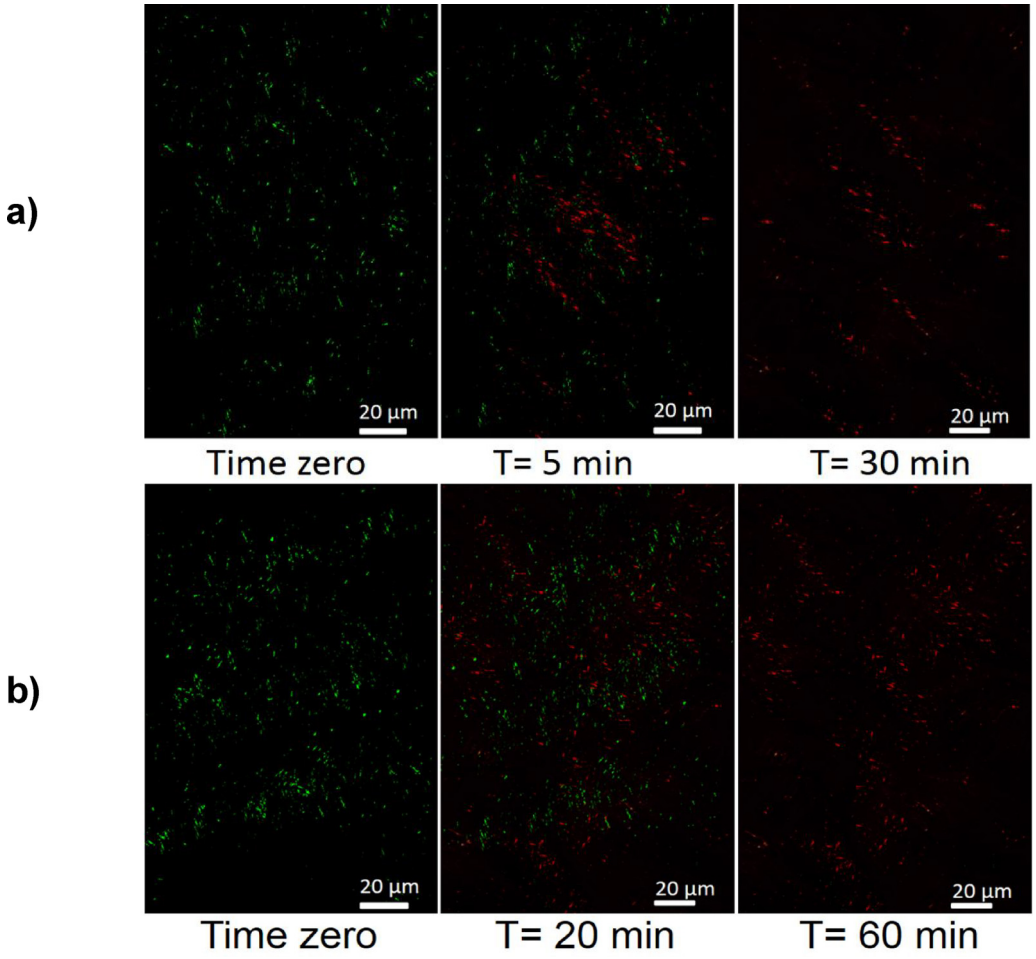

Fig. 6. Live/Dead test of *E. coli* on Cu-PES HIPIMS samples sputtered at 20 A: a) natural *E. coli* K12 ATCC (*omp*R$^+$ *omp*F$^+$*omp*C$^+$), and b) genetically modified *E. coli* TK 821 (*omp*R$^+$ *omp*F$^-$ *omp*C$^-$) under Osram Lumilux 18 W/827 actinic light (4.5 mW/cm^2).

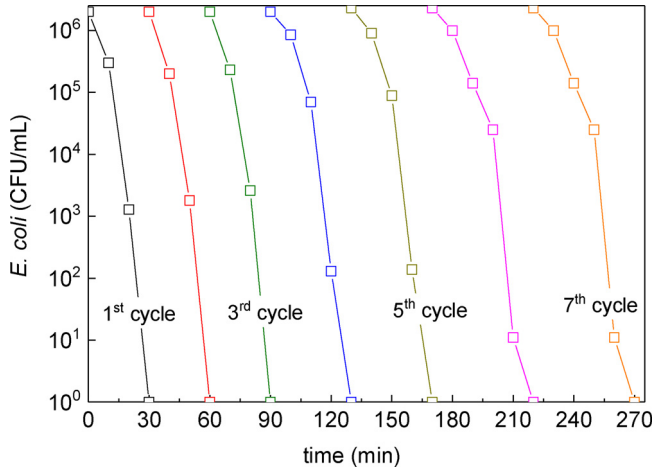

Fig. 7. Recycling of *E. coli* (K 12) inactivation on Cu-PES HIPIMS-sputtered samples at 20 A for 20 s under low intensity actinic light irradiation.

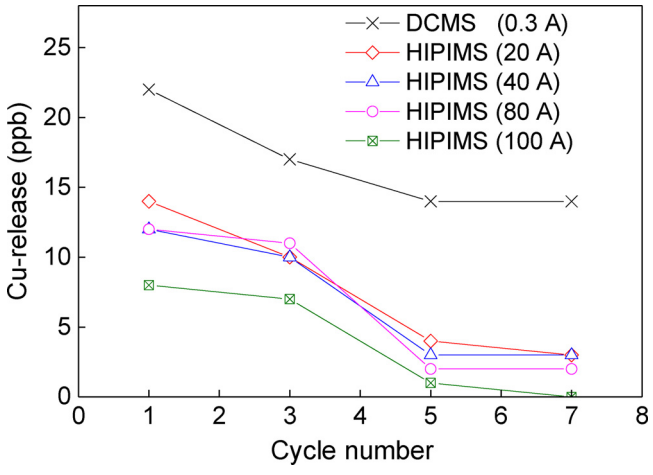

Fig. 8. Cu-ions release during bacterial inactivation cycles of *E. coli* (K 12) determined by ion-coupled plasma mass spectrometry (ICP-MS). Cu-samples as noted in the Figure captions were irradiated under low intensity actinic light (4.5 mW/cm^2).

[66]

$$HO_2\cdot \Leftrightarrow O_2\cdot - + H^+ \; pK_a\ 4.8 \quad (6)$$

The electrostatic interaction between positive Cu-PES with the negatively charged *E. coli* favors the photocatalytic reaction between both species at physiological pH-values. The negative charge of the *E. coli* outer cell bilayers is due to the excess of carboxylic groups of the lipopolysaccharide (LPS) over the amide (I)/(II) groups [3,4,67]. The Cu-PES surfaces are positively charged at physiological pH-values between 6 and 8. The sputtering of Cu on PES builds up CuO/Cu_2O species on the substrate surface as found by XPS measurements and reported in Section 3.5, Fig. 9. The Cu precipitates fully as CuOx/$CuOH_x$ > pH 7.5 and the most common CuO-oxide present an isoelectric point (IEP) of

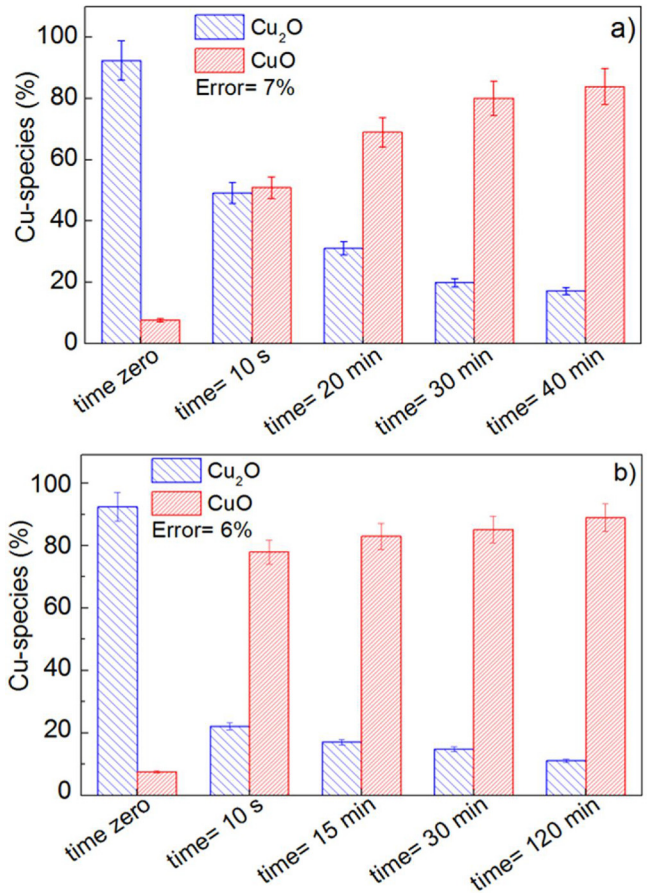

Fig. 9. XPS determination of Cu-oxidative states for samples on The Cu-PES samples leading to *E. coli* bacterial inactivation: a) HIPIMS (20 A), b) DCMS (0.3 A). The times for the selected samples taken for the XPS analyses were in agreement with the bacterial inactivation times reported in Fig. 4.

9.5-10.0. At a pH < 9.5 as used during the bacterial inactivation, the surface of the Cu-PES are positively charged as shown below:

$$CuOH_2^{\delta+} \longleftarrow H^+ + CuOH + OH^- \rightarrow CuO^{\delta-} + H_2O \quad (7)$$

During bacterial inactivation, the pH decreased by 1.2 pH-units (see Fig. 5). The equilibrium at pH > 4.8 is strongly displaced towards the right-hand side (see Eq. (6)) implying the generation of H^+ in solution. The pH-shift is equivalent to an H^+ concentration increase > 10 times. Reaction (2) seems to predominate over reactions (3–4) and reactions (2–3, 5) leading to the generation of HO˚ and HO_2•. These later reactions do not generate species leading to more acidic pH-values.

More important, the Cu-PES is a shorthand notation for CuO/Cu_2O-PES. In the magnetron chamber a residual H_2O vapor (equivalent to 10^{15} molecules/cm^2s or one H_2O-monolayer) is present at Pr = 10^{-4} Pa. The monolayer decomposition produces enough O_2, atomic O and O-ions to oxidize the Cu-NPs to Cu_2O/CuO. Moreover, the Cu-films will be further oxidized to Cu-oxide when the Cu-PES is exposed to air and also after undergoing autoclaving at 121 ˚C [7,22,47].

Stereomicroscopy of the bacterial inactivation of natural *E coli* under actinic light irradiation on Cu-PES samples is shown in Fig. 6a. During the course of the fluorescence stereomicroscopy, the dye enters the cell and stains the cytoplasm DNA (for details see experimental part). The progressive damage/death of the cells as a function of the reaction time is observed in Fig. 6a. Some red dots representing dead bacteria were observed at time zero due to instantaneous bacterial damage/death effect introduced by the Cu-PES samples. The bacterial inactivation kinetics shown in Fig. 6a parallels the data reported in Fig. 5 for the natural *E. coli* bacterial inactivation up to 30 min. Fig. 6b shows that longer times of ~60 min were necessary for the complete bacterial inactivation of the genetically modified porinless bacteria. The *E. coli* ATTC wild bacteria inactivation was faster on the Cu-PES samples compared to the genetically modified *E. coli* bacteria (porinless bacteria). The Cu-ions will translocate/penetrate the *E. coli* ATCC through the normal pores. For the porineless genetically modified *E. coli*, an induction period is required for the surface-contact Cu-cytotoxic effect to take place and damage the bacterial cell wall. This step allows subsequently the Cu-ions to translocate and diffuse into the bacteria cytoplasm but within longer times.

3.4. Recycling of Cu-PES leading to bacterial inactivation and determination of the Cu-ions released by inductively coupled plasma mass spectrometry (ICP-MS)

Fig. 7 present the data for the bacterial inactivation up to the seventh recycling for Cu-PES samples sputtered at 20 A. After each cycle, the Cu-PES samples were washed thoroughly before carrying out the next repetitive recycling. The longer times needed for bacterial inactivation after a few cycles compared with the time reported for the 1st cycle was probably due to the accumulation of bacterial residues on the Cu-PES surface during the inactivation time. These residues did not preclude total bacterial inactivation, but partly block the photocatalyst surface hindering partially the contact between the catalyst surface and bacteria. The first two bacterial inactivation runs needed 30 min each as shown in Fig. 7. The bacterial inactivation kinetics slows down as the number of cycles increased.

Supplementary Fig. S3 reports the same trend for the bacterial inactivation kinetics as shown in Fig. 7 for runs in the dark although occurring at a much slower kinetics.

Fig. 8 shows that the HIPIMS sputtered samples release lower amounts of Cu-ions from the Cu-PES samples compared to samples sputtered by DCMS. HIPIMS sputtered surfaces are more dense and compact compared to DCMS surfaces leading to a lower ion-release. Work addressing this point was recently reported in reference [68]. The more compact HIPIMS sputtered samples in Fig. 8 lead to a slower release of Cu-ions compared to DCMS sputtered samples presenting a lower film density/compactness allowing for a higher release of Cu-ions

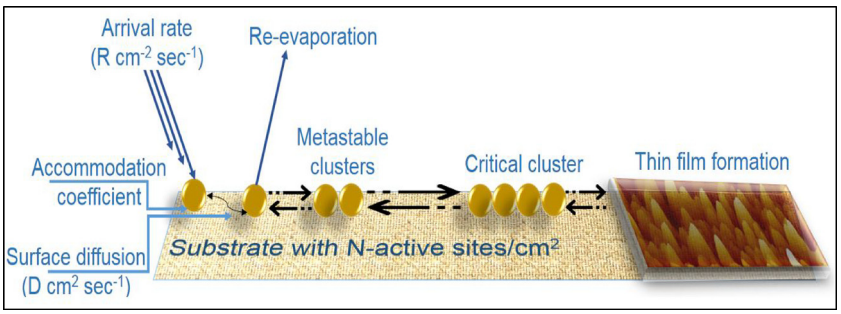

Fig. 10. Suggested scheme for the nucleation of Cu-agglomerates/aggregates/crystals sputtered on PES. See text for further details.

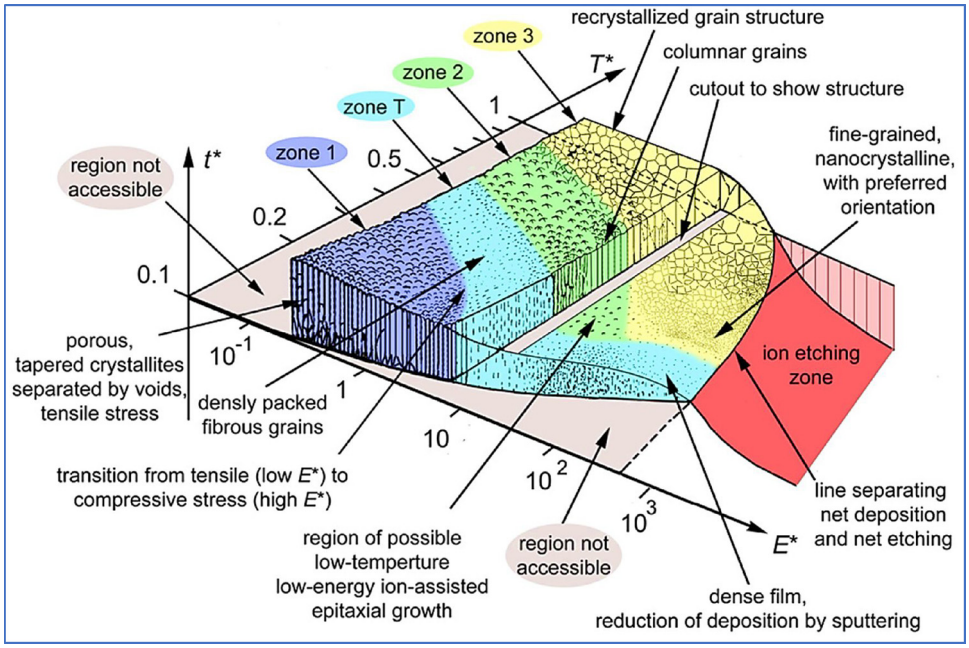

Fig. 11. Structure zone diagram applicable to the deposition energy as suggested by A. Anders (2010). Reproduced from Ref. [76] with Elsevier reproduction rights.

(see Fig. 8).

The low Cu-amounts in the ppb-range detected in Fig. 8 leading to bacterial disinfection suggest that the disinfection may proceed through an oligodynamic effect. The range of Cu released is below the cytotoxic levels permitted by the health regulations for mammalian cells [69–71]. Fig. 7 showed that under actinic light irradiation after the seventh recycling the HIPIMS 20 A photocatalyst was still able to induce complete bacterial inactivation.

Fig. 8 shows that complete bacterial inactivation proceeds not requiring Cu-ions for the HIPIMS (20 A) sample after 7 cycles. This means that the cytotoxicity is induced only by the surface-contact between the Cu-PES and the bacteria cell wall. The bacterial inactivation would proceed through the electrostatic binding/complexation between the Cu-PES positively charged surface and the negative R-S-S-H, N- and COO^- cell wall surface. In this way, a Cu-PES without any release of Cu-ions would degrade the R-S-S-H functional groups leading to cell death [3,5,8].

3.5. Cu-oxide redox states on Cu-PES surfaces followed by X-ray photoelectron spectroscopy (XPS)

Fig. 9a/b presents the change in the Cu(I)O and Cu(II)O species during the bacterial inactivation on HIPIMS and DCMS-coated samples. Both types of sputtering processes induce from the outset Cu(I)O and Cu (II)O-species on the PES surface. The Cu(I)/Cu(II) species were monitored at a later stage during the bacterial inactivation period by XPS. The evolution of the Cu-oxides is shown to follow a different pattern for the HIPIMS and the DCMS prepared samples. At the end of the disinfection period, a ratio of 82% : 18% was observed for the Cu(II)O/Cu(I)O in HIPIMS-samples. The later ratio was 90% : 10% for the DCMS-samples. The different ratio found for both Cu-oxidation states suggests different redox steps occurring during bacterial inactivation. Cu-PES sites transfer the charges induced by light leading to *E. coli* inactivation. This study will not address in detail the bacterial inactivation by Cu(I)O and Cu(II)O-species since this has been widely reported in references [3,5,7,8,22,25,72].

Fig. 10 presents a scheme for the nucleation of the Cu-ions on the surface of the PES. Thin film growth on the PES through nucleation follows involving the formation of atomic clusters which subsequently forms islands which, for long deposition runs, will coalescence and give a continuous film eventually composed of nano-sized crystals of Cu/CuO with different dimensions and growth symmetries [73,38–40,54]. This later step depends on the kinetic energy of the sputtered thin film, the duration of the deposition and, hence on the working parameters during the plasma-based sputtering process. The condensation/coalescence of Cu-ions sometimes lead to the binding to other Cu-atoms rather than to the PES substrate depending on the sputtering parameters applied during the deposition. Cu-chemistry as well as the chemistry of other first row of the transition metals suggest that the elements in this series readily undergo redox reactions with O_2 [74], since the standard redox potential for the $Cu^{1+/2+}$ couple at pH 7 and 25 °C is relatively low at -0.26 V and involves a one electron transfer [75]. A. Anders highlighted the particularities of a thin film deposited in a situation where the film-forming species are ionized and land on the surface while having a rather high kinetic energy, like in a HIPIMS process [76]. Fig. 11 shows a detailed zonation diagram of thin films deposed at different energies. This diagram was established based on three axes: (i) a generalized homologous temperature, (ii) the normalized kinetic energy flux, and (iii) the net film thickness [76].

4. Conclusions

Differentiated *E. coli* bacterial inactivation processes by extracellular and intracellular processes is reported by way of genetically modified bacteria. Plasma analysis, performed though energy-resolved mass analysis highlighted that the Cu-ions produced during the DCMS discharge are less numerous and have a lower kinetic energy with respect to the HIPIMS situation. The bacterial inactivation kinetics induced by Cu-PES samples prepared by these two sputtering processes was evaluated. Insight is provided for the surface-contact and ensuing processes leading to bacterial inactivation. The sample recycling proceeded with a very low Cu-release in the ppb-range. A redox set of reactions for bacterial inactivation is suggested involving Cu(I)/Cu(II) species as detected by XPS. This study contributes to the preparation of more advanced disinfection surfaces showing a potential for practical applications in the treatment of hospital-acquired infections (HAIs) contracted during hospitalization or even short hospital visits. Cu-films sputtered with a low Cu-content were highly cytotoxic, but the cytotoxicity was below the levels inducing mammalian cells damage.

Acknowledgements

This Special Issue is dedicated to honor the retirement of Dr. John Kiwi at the Swiss Federal Institute of Technology (EPFL, Lausanne, Switzerland), a key figure in the topic of photocatalytic materials for the degradation of contaminants of environmental concern. SK is research associate of the Fund for Scientific Research (FNRS, Belgium). VN thanks the Russia Government support (0082-2018-0005 and AAAA-A18-118020690203). SR thanks EPFL.

Appendix A. Supplementary data

Supplementary material related to this article can be found, in the online version, at doi:https://doi.org/10.1016/j.apcatb.2018.08.024.

References

[1] H.H.A. Dollwet, J.R.J. Sorenson, Trace Elem. Med. 2 (1985) 80.
[2] G. Borkow, J. Gabbay, Current. Chem. Biol. 3 (2009) 272.
[3] J. Lemire, J. Harrison, R. Turner, Nature Revs. Microb. 11 (2013) 371–384.
[4] N. Hoiby, T. Bjarnsholt, M. Givskov, S. Molin, O. Ciofu, Int. J. Agents 35 (2010) 322–332.
[5] Byrne J-A, P.S.M. Dunlop, J.W. Hamilton, P. Fernandez-Ibanes, I. Polo-Lopez, P.K. Sharma, A.S.M. Vennard, Molecules 20 (2015) 5574–5612.
[6] J. Schneider, M. Matsuoka, M. Takeuchi, J. Zhang, Yu Horiuchi, M. Anpo, D. Bahnemann, Chem. Revs 4 (2014) 9919–9998.
[7] X. Qiu, M. Miyauchi, K. Sunada, M. Minshima, Min-Liu, Y. Lu, D. Li, Y. Shimodaira, Y. Hosigi, Y. Kuroda, K. Hashimoto, ACS Nano 6 (2012) 1609–1618.
[8] N. Cioffi, N. Ditaranto, L. Torsi, L. Pica, R. Sabatini, A. Valenti, A. Novello, G. Tantillo, T. Bleve-Zacheo, P. Zambonin, Anal. Bioanal. Chem. 381 (2005) 607–616.
[9] J.O. Noyce, H. Michels, C. Keevil, J. Hosp. Infect. 63 (2006) 289–297.
[10] D. Sun, B. Shahzad, M. Li, G. Wang, D. Xu, Mat. Technol: Adv. Biomaterials 30 (2015) B30–B95.
[11] A. Fritsche, M. Haenle, C. Zietz, W. Mittelmeier, G.-H. Neumann, F. Heidenau, B. Finke, R. Bader, J. Mater. Sci. 44 (2000) 5544–5551.
[12] F. Heidenau, F. Mittelmeier, R. Detsch, M. Haenle, M. Gollwitzer, J. Mater. Sci. Mater. Med. 16 (2005) 883–888.
[13] C. Zietz, A. Fritsche, B. Finke, V. Stranak, M. Haenle, R. Hippler, W. Mittelmeier, R. Bader, Bioorg. Chem. Applic. (2012) ID 850390.
[14] R. Plowman, R. Graves, N. Griffin, L. Taylor, Can. J. Infect. Control 47 (2001) 198–204.
[15] A. Kramer, A.I. Schwebke, G. Kampf, Diseases 6 (2006) 137–146.
[16] Dancer, Can. J. Infect. Control 73 (2009) 378–386.
[17] D. Tal, Can. J. Infect. Control 43 (1999) 13–17.
[18] R.M. Klevens, J.R. Edwards, C.L. Richards, T.C. Horan, R.P. Gaynes, D.A. Pollock, D.M. Cardo, Public Health Rep. 122 (2007) 160–166.
[19] K. Page, M. Wilson, I. Parkin, J. Mater. Chem. 12-13 (2005) 2163–12170.
[20] I. Perelshtein, N. Applerot, E. Perkas, E. Wehrshuetz-Sigl, E. Hasman, G. Guebitz, A. Gedanken, Surf. Coat. Technol. 204 (2009) 54–57.
[21] M. Eshed, J. Lellouche, S. Matalon, A. Gedanken, M. Banin, Langmuir 28 (2012) 1228–1234.
[22] D. Quaranta, T. Krans, C. Espirito Santo, C. Elowsky, D. Domaille, C. Chang, G. Grass, Appl. Environ. Microbiol. 77 (2011) 416–426.
[23] C. Espirito Santo, E. Lam, C. Elowsky, C. Quaranta, D. Domaille, C. Chang, G. Grass, Appl. Env. Microb. 77 (2011) 794–802.
[24] C. Espirito Santo, P. Morais, G. Grass, Appl. Env. Microb. 76 (2008).
[25] N. Leyland, A. Podporska, J. Caroll, J. Browne, S. Hinder, B. Quilty, S.C. Pillai, Nature Scientific Repts 6 (2016) 24770–24780.
[26] B. Banerjee, S.C. Pillai, P. Falaras, K. O'Shea, J.-A. Byrne, D. Dionysiou, J. Phys. Chem. Letts 5 (2014) 2543–2554.
[27] M. Fisher, D. Keane, P. Fernandez-Ibanez, J. Colreavy, S. Hinder, K. McGuigan, S.C. Pillai, Appl. Catal. B 130-131 (2013) 8–13.
[28] B. Banerjee, S.C. Pillai, P. Falaras, K. O'Shea, J.-A. Bayrne, D. Dionysiou, J. Phys. Chem. Letts 5 (2014) 2543–2554.
[29] Miguel Pelaez, Nicholas T. Nolan, Suresh C. Pillai, Michael K. Seery, Polycarpos Falaras, Athanassios G. Kontos, Patrick S.M. Dunlop, Jeremy W.J. Hamilton, J.A. Byrne, Kevin O'Shea, Mohammad H. Entezari, Dionysios D. Dionysiou, Appl. Catal. B 125 (2012) 331–349.
[30] C. Gunawan, W. Teoh, C. Marquis, R. Amal, ACS Nano 5 (2011) 7214–7225.
[31] K. Vasilev, J. Cook, J. Griesser, Expert Rev. Medical Devices 6 (2000) 553–567.
[32] O. Akhavan, E. Ghaderi, Surf. Coat. Technol. 205 (2010) 219–223.
[33] T. Yuranova, R. Mosteo, J. Bandara, D. Laub, J. Kiwi, J. Mol. Cat. 244 (2005) 160–167.
[34] G. Borkow, J. Gabbay, J. FASEB 18 (2008) 1728–1730.
[35] G. Borkow, J. Gabba, R. Dadik, A. Eidelman, Y. Lacie, Y. Grinfeld, S. Ikher, M. Husar, R. Zatcoff, R. Marikovsky, Wound Repair Regen. 18 (2010) 266–275.
[36] L.Zhang.R. Dillert, D. Bahnemann, M. Vormoor, En. Environ. Sci. 5 (2012) 7491–7507.
[37] H.A. Foster, W. Sheel, P. Shel, P. Evans, S. Varghese, N. Rutschke, H.M. Yates, J. Photochem. Photobiol. A Chem. 216 (2010) 283–289.
[38] K. Sarakinos, J. Alami, S. Konstantinidis, Surf. Coat. Technol. 204 (2010) 1661–1684.
[39] A. Petrov, M. Myers, J.E. Greene, J.R. Abelson, J. Vac. Sci. Technol. A 12 (1994) 2846–2851.
[40] A.P. Ehiasarian, Pure Appl. Chem. 82 (2010) 1247–1258.
[41] N. Britun, M. Palmucci, S. Konstantinis, R. Snyders, J. Appl. Phys. 117 (2015) 163303.
[42] N. Britun, T. Minea, S. Konstantinidis, R. Snyders, J. Phys. D Appl. Phys. 47 (2014) 224001.
[43] S. Rtimi, Catalysts 7 (2017) 57–67.
[44] S. Rtimi, O. Baghriche, C. Pulgarin, J.-C. Lavanchy, J. Kiwi, Surf. Coat. Technol. 232 (2013) 804–813.
[45] S. Rtimi, C. Pulgarin, J. Kiwi, Coatings 7 (2017) 20–49.
[46] D. Sun, S.A. Crowell, C.M. Hardng, P.M. De Silva, A. Harrison, D.M. Fernando, K.M. Mason, E. Santana, P.C. Loewen, A. Kumar, Y. Liu, Life Sci. 148 (2016) 31–40.
[47] L.C. Seaver, J.A. Imlay, J. Bacter. 183 (2001) 7173–7181.
[48] P. Anthony, P. Pugsley, C. Schnaitman, J. Bacteriol. 133 (1978) 1181–1189.
[49] M. Castro-Alferez, M. Polo-Lopez, P. Fernandez-Ibanez, Sci. Repts. 6 (2016) 38145.
[50] J.F. Moulder, W.F. Stickle, P.E. Sobol, K.D. Bomben, J. Chastain (Ed.), Handbook of X-Ray Photoelectron Spectroscopy, Perkin-Elmer Corporation (Physical Electronics Division), Minnesota, USA, 1992.
[51] J. Nogier, M. Delamar, P. Ruiz, K. Thampi, P. Albers, J. Kiwi, Catal. Today 20 (1994) 109–123.
[52] D.A. Shirley, Phys. Revs. B5 (1972) 4709–4714.
[53] C. Li, X. Tian, C. Gong, J. Xu, Vacuum 133 (2016) 98–104.
[54] V. Kousznetsov, K. Macak, J. Schneider, U. Helmersson, I. Petrov, Surf. Coat. Technol. 122 (1999) 290–293.
[55] A. Brinksman, Sol. Energy Mater. Sol. Cells 827 (1992) 361–368.
[56] M. Lenglet, K. Kartouni, D. Delahaye, J. Appl. Electrochem. 21 (1991) 697–702.
[57] H. Nikaido, J. Biol. Chem. 269 (1994) 3905–3909.
[58] A. Nozik, Annual Rev. Phys. Chem. 29 (1978) 189–206.
[59] P. Docampo, S. Guldin, U. Steiner, J.H. Snaith, J. Phys. Chem. Lett. 4 (2013) 698–703.
[60] N. Kopidakis, R. Neale, K. Zhu, J. van de Lagemaat, J. Frank, Appl. Phys. Letts. 87 (2005) 201106.
[61] Z. Lu, L. Zhou, Z. Zhang, W. Shi, Z. Xie, H. Xie, D. Pang, P. Shen, Langmuir 19 (2003) 8765–8768.
[62] P. Stoimenov, R. Kloinger, G. Marchin, K. Klabunde, Langmuir 18 (2002) 6679–6686.
[63] S. Giannakis, M. Vourmard, S. Rtimi, C. Pulgarin, Appl. Catal. B 227 (2018) 285–295.
[64] J. Fernandez, P. Maruthamuthu, J. Kiwi, J. Photochem. Photobiol. A: Chem. 161 (2004) 185–192.
[65] P. Wardman, J. Phys. Chem. Ref. Data 18 (1989) 1637–1660.
[66] B. Sulzberger, S. Canonica, T. Egli, W. Giger, J. Clausen, U. von Gunten, Chimia 51 (1997) 900–907.
[67] A. Hogt, J. Dankert, J. Freigen, J. Gen. Microbiol. 131 (1995) 2485–2491.
[68] S. Rtimi, S. Giannakis, M. Bensimon, C. Pulgarin, R. Sanjines, J. Kiwi, Appl. Catal. B 191 (2016) 42–52.
[69] O. Bondarenko, K. Juganson, A. Ivask, K. Kasemets, M. Mortimer, A. Kahru, A critical review, Arch. Toxicol. 87 (2013) 1181–1200.
[70] C. Zietz, A. Fritsche, B. Finke, V. Stranak, M. Haenle, R. Hippler, W. Mittelmeier, R. Bade, Bioorg Med Applic. 2012 (2012) 850390.
[71] C. Gunawan, W. Teoh, C. Matrquis, R. Amal, ACS Nano 5 (2011) 7214–7225.
[72] S. Rtimi, M. Robyr, A. Aybush, I. Shelaev, F. Gostev, V. Nadtochenko, J. Kiwi, Appl. Catal. B 20 (2017) 135–147.
[73] I. Mathews, Epitaxial Growth, Part B, IBM Academic Press, New York, NY., USA, 1975, pp. 382–436.
[74] E. Housecroft, C. Constable, Chemistry, 3rd edition, Pearson Ed Ltd, Essex, UK, 2006.
[75] R. Weast, Hanbook of Chem. Phys. 64th ed., CRC Press, Boca Raton, Fla, 1984.
[76] A. Anders, Thin Solid Films 518 (2010) 4087–4090.